Research Article Open Access

Mateus das Neves Gomes, Elizaldo Domingues dos Santos, Liércio André Isoldi, and Luiz Alberto Oliveira Rocha*

Numerical Analysis including Pressure Drop in Oscillating Water Column Device

Abstract: The wave energy conversion into electricity has been increasingly studied in the last years. There are several proposed converters. Among them, the oscillating water column (OWC) device has been widespread evaluated in literature. In this context, the main goal of this work was to perform a comparison between two kinds of physical constraints in the chimney of the OWC device, aiming to represent numerically the pressure drop imposed by the turbine on the air flow inside the OWC. To do so, the conservation equations of mass, momentum and one equation for the transport of volumetric fraction were solved with the finite volume method (FVM). To tackle the water-air interaction, the multiphase model volume of fluid (VOF) was used. Initially, an asymmetric constraint inserted in chimney duct was reproduced and investigated. Subsequently, a second strategy was proposed, where a symmetric physical constraint with an elliptical shape was analyzed. It was thus possible to establish a strategy to reproduce the pressure drop in OWC devices caused by the presence of the turbine, as well as to generate its characteristic curve.

Keywords: Oscillating Water Column (OWC), Numerical Modeling, Volume of Fluid (VOF), Pressure Drop, Turbine

DOI 10.1515/eng-2015-0019
Received January 16, 2015; accepted February 02, 2015

Mateus das Neves Gomes: Paraná Federal Institute of Education, Science and Technology, Paranaguá Campus, Rua Antônio Carlos Rodrigues 453, Porto Seguro, Paranaguá, PR, Brazil
Elizaldo Domingues dos Santos, Liércio André Isoldi: School of Engineering, Universidade Federal do Rio Grande, Cx.P. 474, Rio Grande, RS 96201-900, Brazil
***Corresponding Author: Luiz Alberto Oliveira Rocha:** Department of Mechanical Engineering, Federal University of Rio Grande do Sul, Rua Sarmento Leite, 425, Porto Alegre, RS 90050-170, Brazil, E-mail: luizrocha@mecanica.ufrgs.br

1 Introduction

Nowadays, the investments in exploration of new energy sources are growing, especially in those called renewable energy sources. Renewables are mainly focused on the utilization of solar, wind, biomass and geothermal sources. The diversification of sources should be a target to reach in order to expand and vary the choice [1]. This kind of energy can help to comply with the energetic demand of the world, which had a global energy consumption in 2011 of nearly 1.6×10^7 MW, 60% higher than that consumed in 1980 [2]. So far, the main source of energy to reach this demand has been based on the consumption of fossil fuels. Among several ways to obtain energy from renewable sources, the conversion of the ocean wave energy into electrical power can be an attractive alternative for countries with large coastal regions, such as Brazil.

Ocean energy sources can have different classifications. Undoubtedly, the most relevant are the ocean tidal energy (caused by interaction between the gravitational fields of Sun and Moon), the ocean thermal energy (direct consequence of solar radiation incidence), the ocean currents energy (originated from the gradients of temperature and salinity and tidal action) and, finally, the ocean wave energy (which results from the wind effect over the ocean surface) [3].

The criterion used to classify Wave Energy Converters (WEC), in most references, is associated with the installation depth of the device. In this context, the WECs are classified as: Onshore devices (with access by foot), Nearshore devices (with water depths between 8 and 20 m), and Offshore devices (with water depths higher than 20 m). Other possible classification is related to the main operational principle of the wave energy converters. The main operational physical principles mainly described in literature are: Oscillating Water Column (OWC) devices, Floating Bodies (or surging) devices and Overtopping devices [4].

In the present work, the main operational physical principle of OWC converter is numerically studied. The purpose here is to consider, in the computational model, a physical constraint in the chimney outlet mimicking the effect of

the turbine over the fluid flow inside the OWC device, and its interactions with wave flow. This work will allow future investigations about the turbine influence on the design of an OWC chamber. An analogous approach was already employed by Liu et al. [5]. Moreover, this study has the aim to investigate the employment of two different physical restrictions in the outlet chimney of the OWC chamber. More precisely, the influence of blunt body and elliptical shape restrictions on the available power take off (PTO) is evaluated, in addition to determination of the mass flow rate and pressure drop in the OWC device.

Different dimensions for each kind of physical constraint are tested with the purpose to evaluate the effect of restriction geometry on the ratio between the air mass flow rate crossing the chimney and the internal pressure of the OWC hydropneumatic chamber. For this analysis, the geometrical characteristics of the OWC converter were kept fixed, while the diameter of the physical constraint (d_1) was varied. Hence, it was possible to choose an optimal d_1 value for each kind of constraint. Subsequently, these optimal values were used to study the incidence of a wave spectrum in real scale in the OWC converter, allowing the numerical reproduction of a turbine characteristic curve. In this sense, a strategy to reproduce the pressure drop in OWC devices caused by the presence of the turbine and the generation of the turbine characteristic curve was established.

The computational domains, composed by an OWC inserted into a wave tank, are generated in GAMBIT software. The numerical simulations are performed in FLUENT software, which is a Computational Fluid Dynamic (CFD) package based on the Finite Volume Method (FVM). More details about the FVM can be found in Versteeg and Malalasekera [6]. The Volume of Fluid (VOF) multiphase model was adopted to treat adequately the water-air interaction. The VOF model was developed by Hirt and Nichols [7] and it is already used in other numerical studies related with wave energy (e.g. [8–12]). Furthermore, regular waves are generated in the wave tank, reaching to the OWC converter and generating an alternate air flow through its chimney.

2 Oscillating Water Column (OWC)

The Oscillating Water Column devices are, basically, hollow structures partially submerged, with an opening to the sea below the water free surface, as can be seen in Figure 1. In accordance with Falcão [4], the electricity generation process has two stages: when the wave reaches the structure, the column's internal air is forced to pass through a turbine, as a direct consequence of the augmentation of pressure inside the chamber. When the wave returns to the ocean, the air again passes by the turbine, but now being aspirated from the external atmosphere towards the device chamber, due to the chamber internal pressure decreasing. As a consequence, to enable use of these opposite air movements, the Wells turbine is usually employed, which has the property of maintaining the rotation direction irrespective of the flow direction. The turbine/generator set is responsible for the electrical energy production.

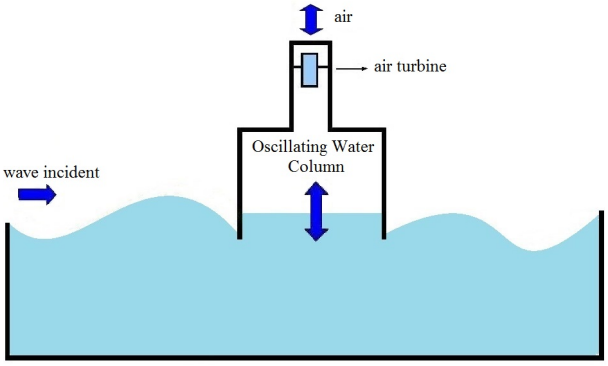

Figure 1: Oscillating Water Column (OWC) converter.

3 Computational domain

As aforementioned, the computational domain consists of the OWC converter inserted into a wave tank. In addition, to represent the pressure drop imposed to the airflow at the OWC, two physical constraints were considered at the chimney device.

Based on the period (T), height (H) and propagation depth (h) of the wave, it is possible to define the length (L_T) and height (H_T) of the wave tank (Figure 2). There is no general rule to establish these dimensions, however some aspects must be taken into account. The wave propagation depth is adopted as the wave tank mean water level, i.e., the wave tank water depth (h). For the wave tank length it is necessary to consider the wave length, as it is recommended that the wave tank length is at least five times the wave length. In this way, a numerical simulation without effects of wave reflection can be performed, during a satisfactory time interval and without an unnecessarily large increase of the computational domain length (which would cause an increase in the computational effort and in the process-

ing time). Regarding the wave tank height, the propagation depth and the height of the wave must be considered. It is suggested to define the wave tank height as equal to the propagation depth plus three times the wave height.

In the first strategy to represent the pressure drop, called constraint A, a blunt body is placed at the OWC chimney, as shown in Figure 3(a). For this case it is expected that a greater influence of the restriction occurs during the air compression, given its geometry is not symmetrical. The geometry employed here is similar to restriction imposed in the previous work of Conde and Gato [13].

The other physical restriction, called constraint B, proposed in this work, has an elliptical geometry, as can be seen in Figure 3(b). Due to its symmetry, the same airflow resistance is caused during compression and decompression stages; this behavior is more realistic when compared with the influence of the Wells turbine.

Some dimensions for the physical constraints were tested, aiming to evaluate the ratio between the air mass flow rate and the pressure inside the OWC hydropneumatic chamber. In this analysis, the geometric characteristics of the OWC device were kept constant, being variable only the diameter (d_1) of the physical constraint. To do so, the optimal geometry obtained by Gomes et al. [14] was adopted, having the follow dimensions: $H_3 = 9.50$ m; $H_1/L = 0.1346$; $L = 16.7097$ m; $H_1 = 2.2501$ m, $l = 2.3176$ m e $H_2 = 6.9529$ m; in addition, a real scale wave (period $T = 5.0$ s, height $H = 1.00$ m, lenght $\lambda = 37.50$ m, and deepth $h = 10.00$ m) was generated.

For the constraint A the dimension d_1 represents its diameter, while the dimension d represents its length (see Figure 3(a)). Analogously, for the constraint B, the dimension d_1 is the ellipse axis lenght in the horizontal direction, while the dimension d defines the ellipse axis lenght in the vertical direction (see Figure 3(b)).

3.1 Boundary Conditions and Mesh

As can be observed in Figure 2, the wave maker is placed in the left side of the wave tank. For the regular wave generation the so-called Function Methodology [15] was employed. This methodology consists of applying the horizontal (u) and vertical (w) components of wave velocity as boundary conditions (velocity inlet) of the computational model, by means of an User Defined Function (UDF) in the FLUENT® software. These velocity components vary as functions of space and time and are based on the Linear Theory of waves. So these wave velocity components are given by:

$$u = \frac{H}{2} gk \frac{\cosh(kz + kh)}{\omega \cosh(kh)} \cos(kx - \omega t) \tag{1}$$

$$w = \frac{H}{2} gk \frac{\sinh(kx + kh)}{\omega \cosh(kh)} \sin(kx - \omega t) \tag{2}$$

where: H is the wave height (m); g is the gravitational acceleration (m/s^2); λ is the wave length (m); k is the wave number, given by $k = 2\pi/\lambda(m-1)$; h is the depth (m); T is the wave period (s); ω is the frequency, given by $\omega = 2\pi/T$ (rad/s); x is the streamwise coordinate (m); t is the time (s); and z is the normal coordinate (m).

Concerning the other boundary conditions, in the upper surfaces of wave tank and chimney and above the wave maker (dashed line in Figure 2) the atmospheric pressure was considered (pressure outlet). In the bottom and right side of computational domain the no slip and impermeability conditions (wall) were adopted.

4 Mathematical model

The analysis consists in finding the solution of a water-air mixture flow. For this, the conservation equations of mass, momentum and one equation for the transport of volumetric fraction are solved via the finite volume method (FVM).

The conservation equation of mass for an isothermal, laminar and incompressible flow with two phases (air and water) is the following:

$$\frac{\partial \rho}{\partial t} + \nabla \cdot (\rho \vec{v}) = 0 \tag{3}$$

where ρ is the mixture density [kg/m^3] and $\vec{v}$ is the velocity vector of the flow [m/s].

The conservation equation of momentum is:

$$\frac{\partial}{\partial t}(\rho \vec{v}) + \nabla(\rho \vec{v}\vec{v}) = -\nabla p + \nabla(\bar{\bar{\tau}}) + \rho \vec{g} + \vec{F} \tag{4}$$

where: p is the pressure (N/m^2), $\rho\vec{g}$ and $\vec{F}$ are buoyancy and external body forces (N/m^3), respectively, and $\bar{\bar{\tau}}$ is the deformation rate tensor (N/m^2), which, for a Newtonian fluid, is given by:

$$\bar{\bar{\tau}} = \mu \left[\left(\nabla \vec{v} + \nabla \vec{v}^T \right) - \frac{2}{3} \nabla \cdot \vec{v} I \right] \tag{5}$$

where μ is the dynamic viscosity (kg/(ms)), and I is a unitary tensor; the second right-hand-side term is concerned with the deviatoric tension (N/m^2).

In order to deal with the air and water mixture flow and to evaluate its interaction with the device, the Volume of

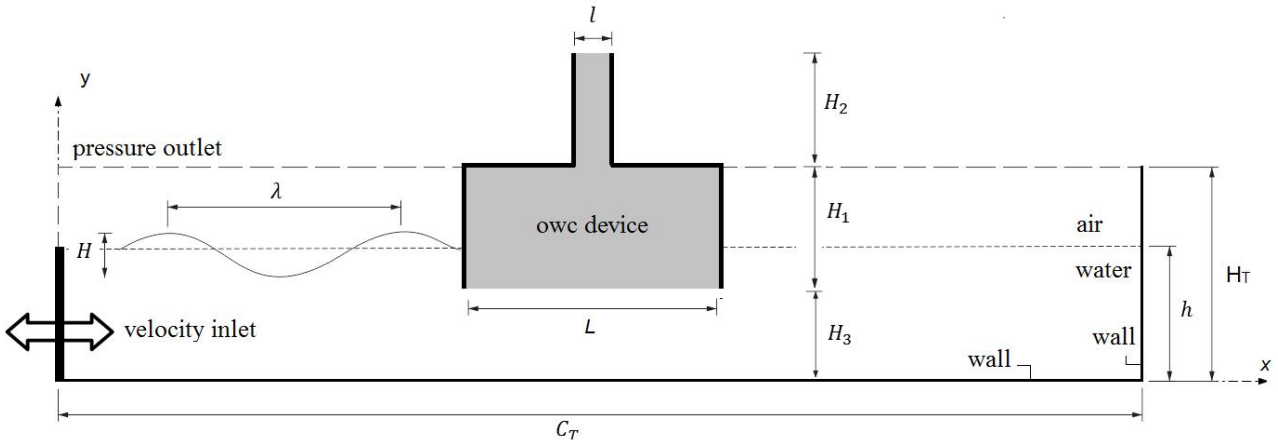

Figure 2: Schematic representation of the computational domain.

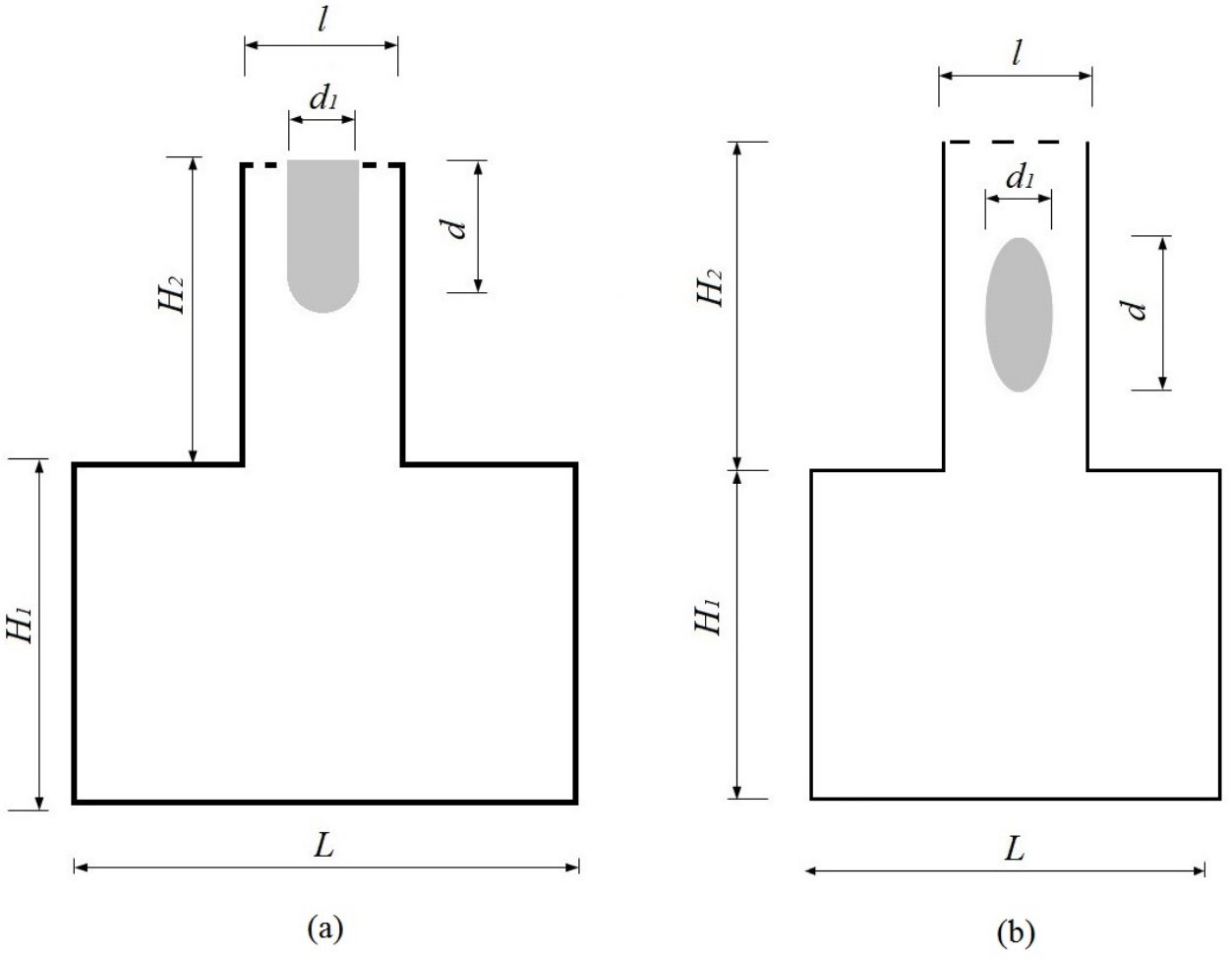

Figure 3: Physical constraints at the OWC chimney: (a) blunt body (constraint A); (b) elliptical body (constraint B).

Fluid (VOF) method is employed. The VOF is a multiphase model used for fluid flows with two or more phases. In this model, the phases are immiscible, i.e., the volume of one phase cannot be occupied by another phase [16, 17].

In the simulations of this study, two different phases are considered: air and water. Therefore, the volume fraction concept (α_q) is used to represent both phases inside one control volume. In this model, the volume fractions are assumed to be continuous in space and time and the sum of volume fractions, inside a control volume, is always unitary ($0 \leq \alpha_q \leq 1$). Consequently, if $\alpha_{water} = 0$, the cell is empty of water and full of air ($\alpha_{air} = 1$), and if the fluid has a mixture of air and water, one phase is the complement of the other, i.e., $\alpha_{air} = 1 - \alpha_{water}$. Thus, an additional transport equation for one of the volume fractions is required:

$$\frac{\partial(\rho\alpha_q)}{\partial t} + \nabla \cdot \left(\rho\alpha_q\vec{v}\right) = 0 \tag{6}$$

It is worth mentioning that the conservation equations of mass and momentum are solved for the mixture. Therefore, it is necessary to obtain values of density and viscosity for the mixture, which can be written by:

$$\rho = \alpha_{water}\rho_{water} + \alpha_{air}\rho_{air} \tag{7}$$

$$\mu = \alpha_{water}\mu_{water} + \alpha_{air}\mu_{air} \tag{8}$$

5 Numerical model

For the numerical simulation of the conservation equations of mass and momentum, a commercial code based on the FVM is employed [18]. The solver is pressure-based and all simulations were performed using 'upwind' and PRESTO for spatial discretizations of momentum and pressure, respectively. The velocity-pressure coupling is performed by the PISO method, while the GEO-RECONSTRUCTION method is employed to tackle with the volumetric fraction. Moreover, under-relaxation factors of 0.3 and 0.7 are imposed for the conservation equations of continuity and momentum, respectively. More details concerning the numerical methodology can be obtained in the works of Versteeg and Malalasekera [6] and Patankar [19]. The numerical simulations were performed using a computer with two dual-core Intel processors with 2.67 GHz clock and 8 GB ram memory. It used Message Passing Interface (MPI) for parallelization. The processing time of each simulation was approximately two hours.

It is important to emphasize that this numerical methodology was already validated in previous studies of this research group [14, 15]. Therefore, for the sake of brevity, this validation will not be repeated in this study.

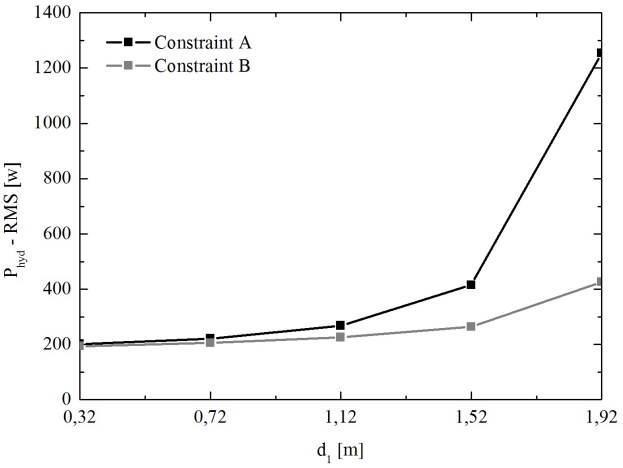

Figure 4: The effect of diameter (d_1) over the RMS available hydropneumatic power for the two different studied constraints.

6 Results and Discussions

Five values for the dimension d_1 were tested (Table 1), for both constraints (A and B). For the constraint A, the value of d was also changed, being considered $d = 1$ m plus the constraint radius ($d_1/2$) for each case. For the constraint B the value of d is constant, as noted in Table 1.

Figure 4 shows the effect of physical constraint diameter (d_1) over the root mean square (RMS) hydropneumatic power (P_{hyd}) for constraints A and B. For constraint A it can be noticed that the increase of d_1 leads to an increase of $P_{hyd-RMS}$ in the device, especially for $d_1 \geq 1.1176$ where the magnitude of P_{hyd} had a step increase. For constraint B, results showed an increase of P_{hyd} with the increase of the diameter of the restriction (d_1). However, the increase of P_{hyd} for constraint B is smoothed in comparison with those reached for constraint A, especially in the range $1.1176 \leq d_1 \leq 1.9176$, where the highest magnitudes of P_{hyd} are achieved for both constraints. In other words, results showed that the employment of different geometries for each constraint also led to differences in available power in the OWC device.

With the purpose to improve the comprehension about the effect of d_1 over the available power of the device, the transient mass flow rate for constraints A and B (Figure 5(a) and Figure 5(b)), as well as transient pressure inside the chamber for the same constraints (Figure 6(a) and Figure 6(b)) are shown.

Table 1: Physical constraint dimensions.

Case	Constraint A			Constraint B		
	d_1[m]	d [m]	Area [m^2]	d_1[m]	d [m]	Area [m^2]
0	0.0000	0.0000	0.0000	0.0000	0.0000	0.0000
1	0.3176	1.1588	0.3968	0.3176	2.0000	0.4988
2	0.7176	1.3588	1.1220	0.7176	2.0000	1.1272
3	1.1176	1.5588	2.0985	1.1176	2.0000	1.7555
4	1.5176	1.7588	3.3264	1.5176	2.0000	2.3838
5	1.9176	1.9588	4.8056	1.9176	2.0000	3.0121

For constraint A, a decrease of mass flow rate for every instants of time with the augmentation of geometrical constraint can be seen (Figure 5(a)). This effect is more evident for constraint case 5, where a reduction of nearly 30% is noticed for the mass flow rate. Concerning the pressure inside the chamber, Figure 6(a) shows a strong increase of pressure inside the chamber with the augmentation of the restriction. For instance, for $t = 27.0$ s, the pressure increases four times from restriction case 4 to restriction case 5. In this sense, the increase of pressure gradient from the chamber to the chimney outlet for the case with the largest restriction compensates the decrease of mass flow rate. It is worthy to mention that a minimal momentum for the air flow is required to drive the turbine. As a consequence, the imposition of a turbine with large turbine hub diameter (d_1) can be inviable in practical applications.

For constraint B, results of mass flow rate (Figure 5(b)) show that the elliptical restriction leads to similar magnitudes for all values of d_1 investigated, with slight differences in peaks and values of mass flow rate. Concerning the pressure inside the chamber, for constraint B (Figure 6(b)) the magnitude of pressures are similar in the inlet and outlet of the air flow in the device, which is not noticed for constraint A. This difference can be assigned to differences in the geometrical shape of constraints A and B. In constraint A the geometry is asymmetric and inserted in the chimney outlet, while constraint B is symmetric and inserted in the center of chimney leading to a more symmetrical behavior of pressure inside the chamber.

In general, the results of power as a function of diameter d_1 show the importance of geometrical evaluation of turbine inserted in the OWC chimney. For constraint A, the highest diameter d_1 evaluated leads to an available power six times higher than that achieved with the lowest diameter d_1 studied. For both cases (constraints A and B) the highest value of d_1 leads to the highest available power in the device. However, for constraint A and $d_1 > 1.5176$ m the mass flow rate suffers a strong decrease. Moreover, the

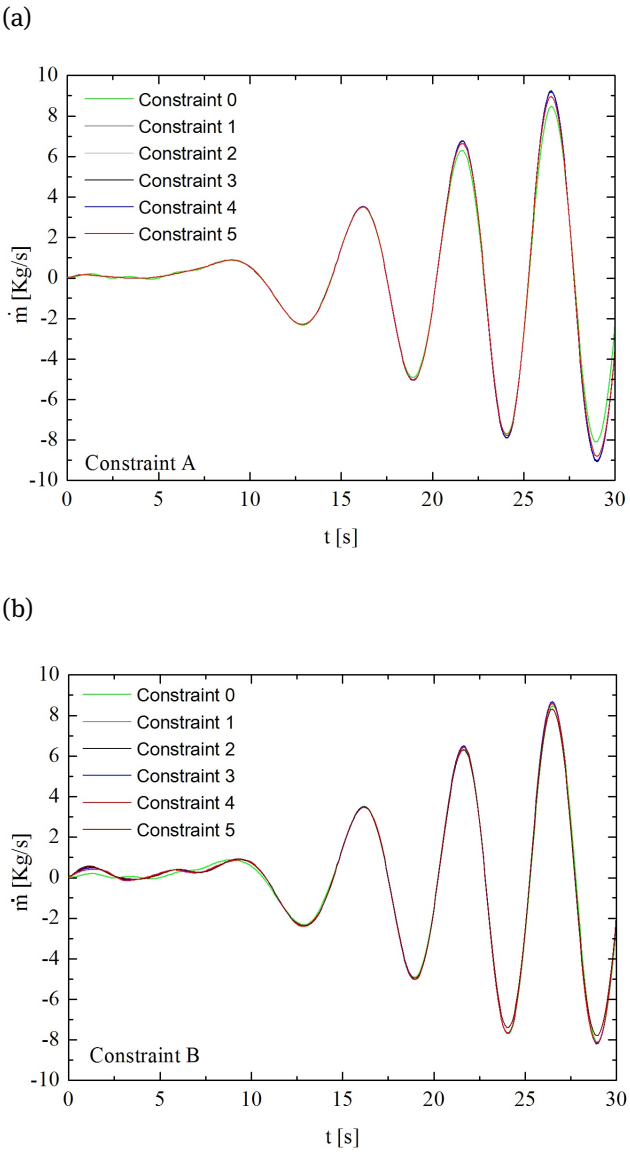

Figure 5: Transient behavior of mass flow rate for all studied diameters (cases 0 to 5, see Table 1) for: (a) constraint A; (b) constraint B.

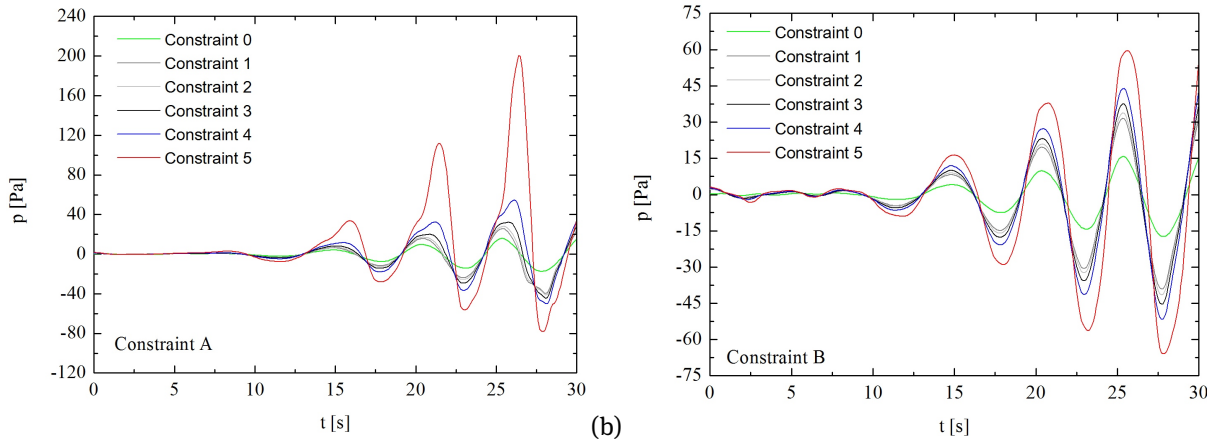

Figure 6: Transient behavior of pressure inside the chamber for all studied diameters (cases 0 to 5, see Table 1) for: (a) Constraint A; (b) Constraint B.

pressure inside the chamber increases dramatically, being necessary to decrease the pressure inside the chamber by means of a by-pass valve in the OWC chamber.

Weber and Thomas [20] presented three dimensionless coefficients for the mass flow rate (flow coefficient), for the pressure drop (pressure coefficient) and for the available power (power coefficient). The effect of pressure coefficient (ψ) over the flow coefficient (ϕ) and power coefficient (Π) has been described in literature, mainly into the experimental framework [20].

Figure 7(a) shows the effect of pressure coefficient over the flow coefficient, and Figure 7(b) depicts the effect of pressure coefficient over the power coefficient. As aforementioned, these curves are constructed by means of simulation of a wave spectrum for a pre-determined restriction ($d_1 = 1.5176$ m, which represents a condition where the fluid flow inside the chamber does not suffer a strong reduction of mass flow rate nor a strong increase of pressure inside the chamber). The results showed an almost linear relation between the pressure coefficient and flow coefficient, which represents adequately the characteristic curve of a Wells turbine. For power coefficient, the behavior is also almost linear, except in regions of highest pressure where the power begins to decrease. In general, the behavior predicted numerically is similar to those obtained experimentally in existing literature [20]. In this sense, the employment of a restriction mimicking the effect of a turbine over the fluid flow seems an adequate methodology to construct the characteristic turbine curve for an OWC device.

7 Concluding remarks

In the present work, a numerical study was performed with the purpose of comparing the imposition of two different physical restrictions at the chimney outlet, mimicking the effect of a turbine over the fluid flow inside an OWC chamber device. The first strategy considered a bluff body in the chimney outlet (constraint A) and the second approach imposed an elliptical obstacle (constraint B) in the half of chimney duct. The effect of geometry on the available power take off in the device is evaluated. Subsequently, the best geometries were submitted to wave flows under different conditions in order to generate a turbine characteristic curve. The conservation equations of mass, momentum and the volumetric fraction were solved with the employment of a CFD package based on the Finite Volume Method. To treat the interaction between the water-air mixture, the Volume of Fluid (VOF) method was used.

Results showed that the type of restriction affected the available power as well as the transient behavior of the air flow inside the chamber. On the one hand, constraint B (elliptic form) led to similar magnitudes of mass flow rate and pressure drop in the exhaustion and suction of the air into the chamber. On the other hand, for constraint A (bluff body), the pressure inside the chamber behaved in an asymmetric way, with higher pressure drop magnitudes in the exhaustion than in the suction of the air through the chimney. It was also noticed that two main factors must be taken into account to represent adequately the turbine by means of an imposed restriction: the pressure inside the chamber and the mass flow rate. The combination of these two parameters generated the available power in the device.

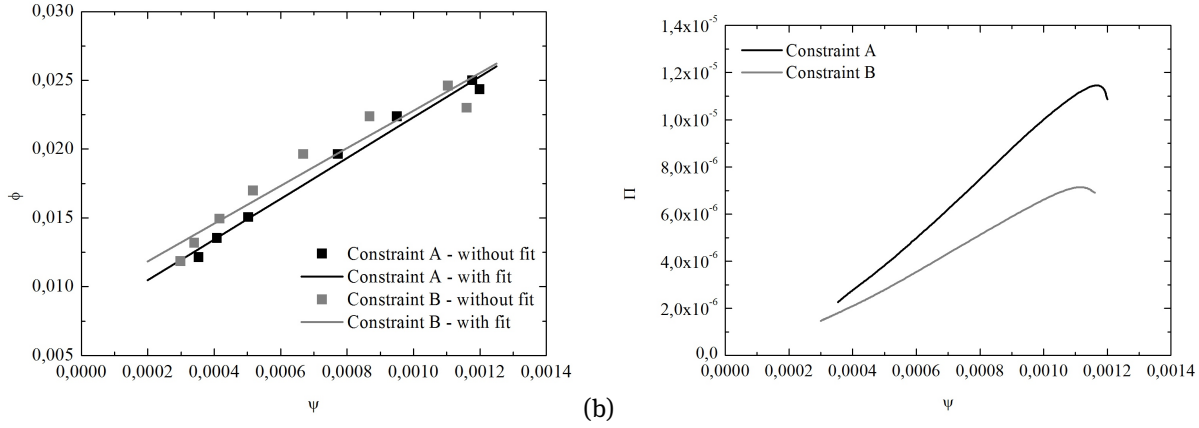

Figure 7: Wells characteristic curves represented by constraints A and B: (a) flow coefficient (ϕ) as a function of pressure coefficient (ψ); b) power coefficient (Π) as a function of pressure coefficient.

The effect of restriction geometry, more precisely the parameter d_1, on the available power in the OWC device was also evaluated. The parameter d_1 had a strong influence on the available power in the OWC chimney. For constraint A, for example, the largest diameter d_1 evaluated led to an available power six times greater than that achieved with the lowest diameter d_1 studied. Results allowed the determination of a theoretical recommendation for the parameter d_1, which must be increased until a superior limit is reached, where the momentum is enough to drive the turbine, and where the pressure inside the chamber is not large enough to supress the water movement inside the chamber.

Lastly, the optimal value of d_1 that maximizes the available power and at the same time does not cause a strong reduction in the mass flow rate and excessive pressure inside the chamber was used to study the incidence of a wave spectrum in real scale in the OWC converter, allowing the construction of a turbine characteristic curve. In this sense, it was possible to establish a strategy to reproduce the pressure drop in OWC devices caused by the presence of the turbine and to generate its characteristic curve, as well as estimate the available power in the device. The behavior found numerically here was similar to those obtained experimentaly in literature [20]. Future studies will use this methodology for geometric optimization of device chamber.

Acknowledgement: The authors thank the Universidade Federal de Rio Grande (FURG), Universidade Federal do Rio Grande do Sul (UFRGS), Instituto Federal do Paraná (IFPR), FAPERGS and CNPq (Process: 555695/2010-7) for financial support. E. D. dos Santos, L. A. Isoldi and L.A.O. Rocha also thank CNPq for a research grant and E. D. dos Santos thanks FAPERGS for financial support (Process: 12/1418-4).

Conflict of Interest

The authors do not have a direct financial relation with the commercial identity mentioned in this paper, avoiding any conflict of interest.

Nomenclature

d	Length of constraint [m]
d_1	Diameter of the constraint [m]
$\vec{F}$	External body forces [N/m^3]
g	Gravitational acceleration [m/s2]
h	Propagation depth [m]
H	Wave height [m]
H_1	Height of the chamber [m]
H_2	Height of the chimney [m]
H_3	Lip submergence [m]
H_T	Height of the wave tank [m]
I	Unitary tensor tension [N/m^2]
k	Wave number [m^{-1}]
l	Length of the chimney [m]
L	Length of the chamber [m]
L_T	Length of the wave tank [m]
p	Pressure [Pa]
P_{hyd}	Hydropneumatic power [W]
t	Time [s]
T	Wave period [s]
u	Horizontal component of the velocity of the wave [m/s]
v	Vertical component of the velocity of the wave [m/s]

$\vec{v}$ Velocity vector [m/s]
x Streamwise coordinate [m]
z Normal coordinate [m]

Greek Letters

α Volume fraction [dimensionless]
λ Wave length [m]
μ Dynamic viscosity [Kg/ms]
ρ Mixture density [Kg/m^3]
$\overline{\overline{\tau}}$ Deformation rate tensor [N/m^2]
Π Power coefficient [dimensionless]
ω Frequency [rad/s]
ϕ Flow coefficient [dimensionless]
ψ Pressure coefficient [dimensionless]

Acronyms

CFD Computational Fluid Dynamics
FVM Finite Volume Method
MPI Message Passing Interface
OWC Oscillating Water Column
PISO Pressure-Implicit with Splitting of Operators
PTO Power Take Off
RMS Root Mean Square
VOF Volume Of Fluid
WEC Wave Energy Converters

References

[1] A. F. Miguel, M. Aydin. Ocean exergy and energy conversion systems. Int. J. of Exergy 10 (2013) 454-470.
[2] F. Zabihian, A.S. Fung, Review of marine renewable energies: case study of Iran, Renew. Sust. Energ. Rev. 15 (2011) 2461-2474.
[3] R. Pelc, R. M. Fujita, Renewable energy from the ocean. Marine Policy 26 (2002) 471-479.
[4] A. F.de O. Falcão. Wave energy utilization: A review of the technologies. Renewable and Sustainable Energy Reviews. 14 (2010) 899-918.
[5] Z. Liu, B. S. Hyun, K. Hong, Y. Lee, Investigation on integrated system of chamber and turbine for OWC wave energy convertor, Proceeding of the nineteenth international offshore and polar engineering conference (2009), 276-282.
[6] H. K. Versteeg, W. Malalasekera, An Introduction to Computational Fluid Dynamics – The Finite Volume Method, Longman, England, 1995.
[7] C. W. Hirt, B. D. Nichols, Volume of fluid (VOF) method for the dynamics of free boundaries, Journal of Computational Physics, 39 (1981), 201-225.
[8] M. Horko, CFD Optimization of an oscillating water column energy converter, MSc. Thesis, School of Mechanical Engineering, The University of Western, Australia, 2007.
[9] Z. Liu, B.-S. Hyun, K. Hong, Numerical study of air chamber for oscillating water column wave energy /convertor, China Ocean Eng. 25 (2011) 169-178.
[10] M. das N. Gomes, Computational modeling of an Oscillating Water Column device to conversion of wave energy into electrical energy (in Portuguese), MSc. Thesis, Federal University of Rio Grande, Brazil, 2010.
[11] E.D. Dos Santos, B.N. Machado, N.R. Lopes, J.A. Souza, P.R.F. Teixeira, M.N. Gomes, L.A. Isoldi, L.A.O. Rocha, Constructal Design of Wave Energy Converters, in: L.A.O. Rocha, S. Lorente, A. Bejan (Eds.), Constructal Law and the Unifying Principle of Design, Springer, New York, 2013, pp. 275-294.
[12] E. D. dos Santos, B. N. Machado, M. M. Zanella, M. das N. Gomes, J. A. Souza, L. A. Isoldi, L. A. O. Rocha, Numerical Study of the Effect of the Relative Depth on the Overtopping Wave Energy Converters According to Constructal Design. Defect and Diffusion Forum 348 (2014) 232-244.
[13] J. M. P. Conde, L. M. C. Gato, Numerical study of the air-flow in na oscillating water column wave energy converter. Renew. Energy 33 (2008) 2637 – 2644.
[14] M. N. Gomes, M, E. D. dos Santos, E, L. A. Isoldi, L. A. O. Rocha, Two-dimensional geometric optimization of an oscillating water column converter of real scale, Proceedings 22nd International Congress of Mechanical Engineering, COBEM, (2013), Ribeirão Preto.
[15] M. das N. Gomes, C.R. Olinto, L.A.O. Rocha, J.A. Souza, L.A. Isoldi, Computational modeling of a regular wave tank. Therm. Eng. 8 (2009) 44-50.
[16] L. Ling, C. Yongcan, L. Yuliang, Volume of fluid (VOF) method for curved free surface water flow in shallow open channel, Department of Hydraulic Engineering, Tsinghua University, Beijing, 2001.
[17] X. Lv, Q. Zou, D. Reeve, Numerical simulation of overflow at vertical weirs using a hybrid level set/VOF method, Adv. Water Resour. 34 (2011) 1320-1334.
[18] FLUENT, version 6.3.16, ANSYS Inc., 2007.
[19] S.V. Patankar, Numerical Heat Transfer and Fluid Flow, McGraw Hill, New York, 1980.
[20] J. W. Weber, G. P. Thomas, An investigation into the importance of the air chamber design of an oscillating water column wave energy device, Proceeding of the eleventh international offshore and polar engineering conference (2001), pp. 581-588.